Role of target geometry in phagocytosis

Julie A. Champion and Samir Mitragotri[†]

Department of Chemical Engineering, University of California, Santa Barbara, CA 93106

Communicated by Jacob N. Israelachvili, University of California, Santa Barbara, CA, February 6, 2006 (received for review October 11, 2005)

Phagocytosis is a principal component of the body's innate immunity in which macrophages internalize targets in an actin-dependent manner. Targets vary widely in shape and size and include particles such as pathogens and senescent cells. Despite considerable progress in understanding this complicated process, the role of target geometry in phagocytosis has remained elusive. Previous studies on phagocytosis have been performed using spherical targets, thereby overlooking the role of particle shape. Using polystyrene particles of various sizes and shapes, we studied phagocytosis by alveolar macrophages. We report a surprising finding that particle shape, not size, plays a dominant role in phagocytosis. All shapes were capable of initiating phagocytosis in at least one orientation. However, the local particle shape, measured by tangent angles, at the point of initial contact dictates whether macrophages initiate phagocytosis or simply spread on particles. The local shape determines the complexity of the actin structure that must be created to initiate phagocytosis and allow the membrane to move over the particle. Failure to create the required actin structure results in simple spreading and not internalization. Particle size primarily impacts the completion of phagocytosis in cases where particle volume exceeds the cell volume.

drug delivery | macrophages | membrane | shape

Phagocytosis is a principal component of the body's innate immunity in which macrophages and other antigen-presenting cells internalize large (>0.5 μm) particulate targets (1). Examples of targets include pathogens such as rod-shaped *Escherichia coli* and *Bacillus anthracis* and spiral-shaped *Campylobacter jejuni*, disk-shaped senescent cells such as aged erythrocytes, and airborne particles such as dust and pollen, all of which vary widely in both shape and size. Because macrophages in the human body encounter targets with such diversity, the question has long been asked, how does target geometry impact phagocytosis? Several studies have been conducted specifically to address this question; however, a generalized answer is still lacking. The main reason behind this shortcoming is that all phagocytosis studies have been performed with spherical targets (2–7). Exclusive use of spherical particles originated partly because of a presumption that size is the principal parameter of interest and partly because of difficulties in fabricating nonspherical particles of controlled dimensions. Use of spherical particles not only concealed the role of particle shape in phagocytosis but also created an inaccurate picture of the actual role of particle size because all parameters that describe size (volume, surface area, etc.) scale with particle radius, leaving one wondering as to which parameter is of fundamental consequence in phagocytosis. Accordingly, the precise roles of target size and shape in phagocytosis, despite their high relevance, remain largely unknown.

Herein, we report, using alveolar macrophages as model phagocytes and polystyrene (PS) particles of various sizes and shapes as model targets, that target shape at the point of first contact by macrophages, not size, decisively determines whether cells will proceed with phagocytosis or simply spread on the particle. Size, on the other hand, primarily impacts the completion of phagocytosis when the target volume is larger than the macrophage volume.

Results and Discussion

We designed an array of nonopsonized and IgG-opsonized geometrically anisotropic PS particles and studied their phagocytosis by alveolar macrophages. PS was chosen for its ability to be manipulated with heat and solvent, allowing a wide range of tunable shape characteristics such as aspect ratio, size, concavity, and curvature to be applied to the particles. The particles were created to probe the role of shape, not necessarily to mimic natural phagocytic targets. The results obtained for PS particles should not be directly extrapolated to natural targets. Particles representing six distinct geometric shapes were fabricated (Fig. 1 *A–F*): spheres (radius 1.0–12.5 μm), oblate ellipsoids (major axis 4 μm, aspect ratio 4), prolate ellipsoids (major axis 2–6 μm, aspect ratio 1.3–3), elliptical disks (EDs) (major axis 3–14 μm, aspect ratio 2–4, thickness 400–1,000 nm), rectangular disks (major axis 4–8 μm, aspect ratio 1.5–4.5), and UFOs (sphere radius 1.5 μm, ring radius 4 μm). Fabrication of these particles is a challenge in itself and has not been reported in the literature except in the case of prolate ellipsoids (8, 9).

Opsonized or nonopsonized particles were incubated with alveolar macrophages and observed under a light microscope ($\times$100) with time-lapse video microscopy. IgG-opsonized particles are phagocytosed via Fc receptors (1, 10), whereas nonopsonized particles adsorb proteins from the culture medium supplemented with heat-inactivated FBS during incubation and are phagocytosed through nonspecific scavenger receptors (11, 12). In both cases internalization of particles is an actin-dependent process (1, 13).

Internalization of both opsonized and nonopsonized particles exhibited a strong dependence on local particle shape from the perspective of the phagocyte. Local shape varies not only for different particles but also for different points of initial contact on the same particle, except for spheres. For example, macrophages that attached to EDs (major axis 14 μm, minor axis 3 μm) along the major axis (discussed quantitatively below) internalized them very quickly, in <6 min (Fig. 2*A*; and see Movie 1, which is published as supporting information on the PNAS web site). The macrophage membrane can be seen moving along the length of the particle in a coordinated, unified fashion. On the other hand, cells that attached to the same EDs along the minor axis or flat side did not internalize them, even after 2 h (Fig. 2*B*; and see Movie 2, which is published as supporting information on the PNAS web site). They did, however, spread on the particle surface but with nonsynchronized, separate fronts moving in different directions at different times. Macrophages attached to the flat side of IgG-opsonized EDs exhibited more spreading than those attached to nonopsonized EDs, but the final result was the same: no phagocytosis. Because the particles used for these studies possessed identical properties (dimensions, surface area, volume, and chemistry), observations in Fig. 2 *A* and *B* clearly show that the local particle shape at the point of initial contact, not the overall size, determined their phagocytic fate. Similar results were seen for all shapes including UFO-shaped

Conflict of interest statement: No conflicts declared.

Abbreviations: ED, elliptical disk; PS, polystyrene; PVA, poly(vinyl alcohol).

[†]To whom correspondence should be addressed. E-mail: samir@engineering.ucsb.edu.

www.pnas.org/cgi/doi/10.1073/pnas.0600997103

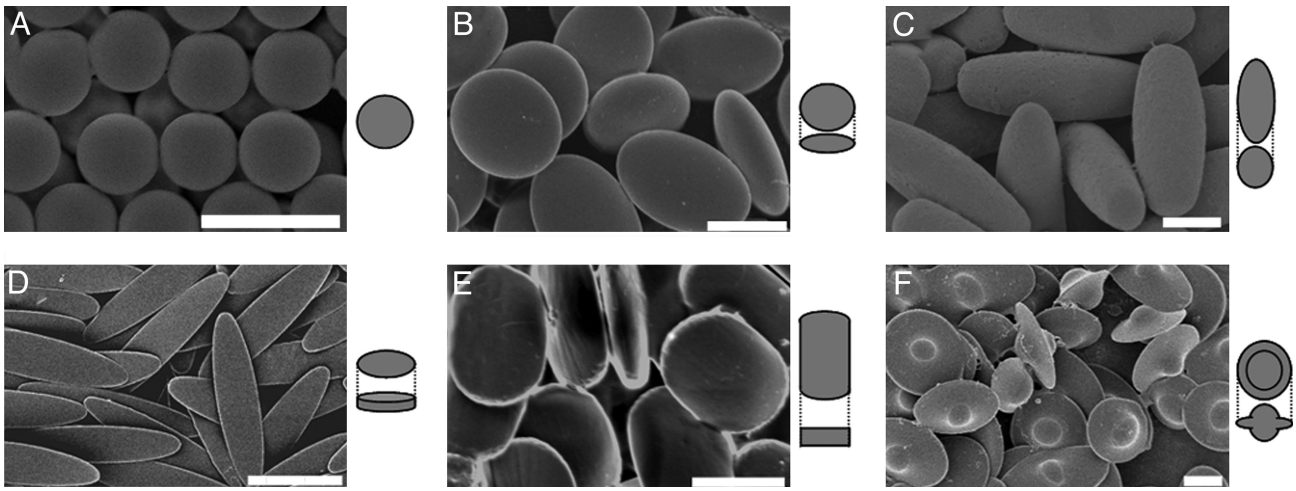

Fig. 1. Scanning electron micrographs and 3D illustrations of PS particles created for phagocytosis experiments. (*A*) Spheres. (*B*) Oblate ellipsoids (13%). (*C*) Prolate ellipsoids (7%). (*D*) Elliptical disks (9%). (*E*) Rectangular disks (5%). (*F*) UFOs (12%). Particles are monodispersed with average standard deviations of measured dimensions for each shape listed in parentheses. A portion of this variation is due to 2–5% standard deviation in the diameter of spheres used as starting materials. (Scale bars: 5 μm.)

particles, where internalization does not occur when cells attach to the concave region but internalization does occur after attachment to the dome or ring regions.

Scanning electron microscopy images provided more evidence for this orientation bias. As can be seen in the micrographs, the cell membrane showed marked progression on EDs when approached along the major axis (Fig. 3*A*). In contrast, cells that attached to the flat side of EDs exhibited spreading but no engulfment of particles, even after 2 h (Fig. 3*B*). As a reference point, consistent engulfment was observed on spheres (Fig. 3*C*).

Further insight into orientation-dependent particle phagocytosis was gained by staining macrophages for polymerized actin at various times during phagocytosis. Actin polymerization is the principal mechanism by which macrophages push the leading membrane edge and engulf particles (13). Initially, an actin cup, comprised of a dense actin network, forms beneath the particle. As additional actin polymerization and remodeling occur and the membrane progresses, the actin cup is transformed into an actin ring around the particle that pushes the membrane along the particle until it is internalized (14–16). Spheres and EDs that attached to macrophages along the major axis exhibited an actin cup at short times that later transformed to a ring around the particle as phagocytosis progressed (Fig. 3 *F* and *D*, respectively). Macrophage attachment to the flat side of EDs, despite actin polymerization at points of contact and spreading, did not exhibit an actin cup or ring (Fig. 3*E*). Formation of an actin cup is a clear indicator of initiation of internalization and was observed only at certain local shapes.

To arrive at a generalized and quantitative statement about the role of shape in phagocytosis, we defined the angle Ω between the membrane normal at the point of initial contact, $\bar{\mathbf{N}}$, and a vector $\bar{\mathbf{T}}$ whose angle represents the mean direction of

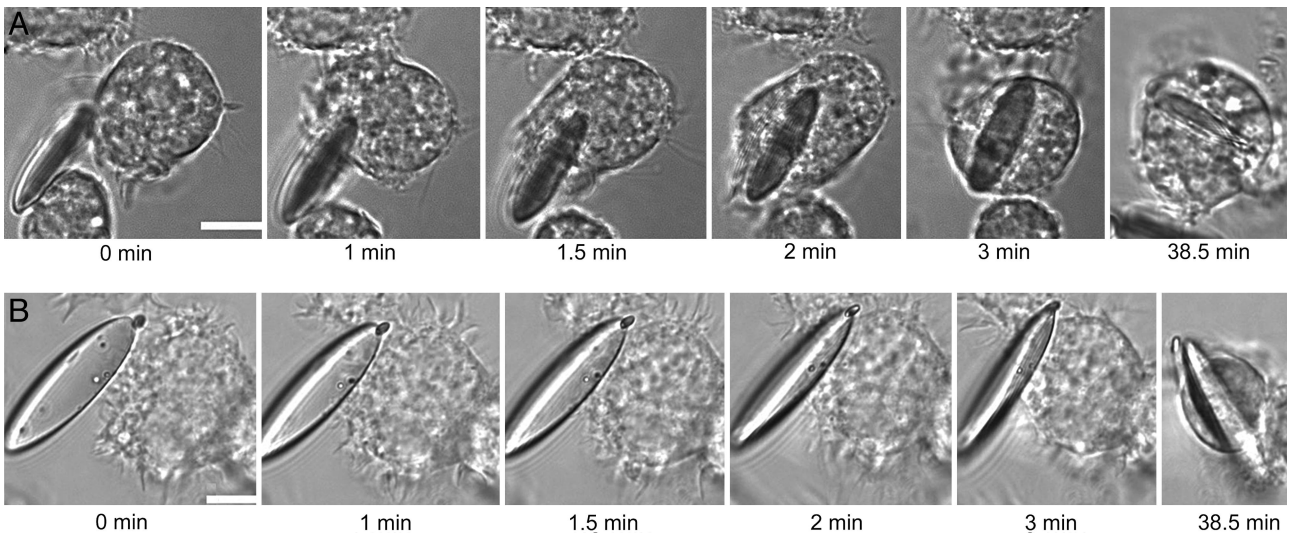

Fig. 2. Time-lapse video microscopy clips spanning 39 min of macrophages interacting with identical nonopsonized ED particles (major axis 14 μm, minor axis 3 μm) from two different orientations. (*A*) Cell attaches along the major axis of an ED and internalizes it completely in 3 min. (*B*) Cell attaches to the flat side of an identical ED and spreads but does not internalize the particle. Continued observation indicated that this particle was not internalized for >110 min. (Scale bars: 10 μm.) (See Movies 1 and 2.) At least three cells were observed for each orientation of each particle type and size. Similar results were observed in all repetitions.

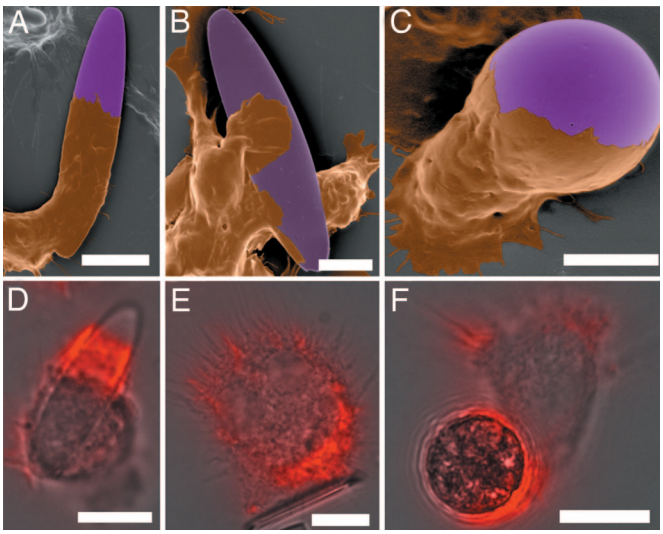

Fig. 3. Scanning electron micrographs and actin staining confirm time-lapse video microscopy observations. Micrographs (*A–C*) of cells and particles were colored brown and purple, respectively. (*A*) The cell body can be seen at the end of an opsonized ED, and the membrane has progressed down the length of the particle. (Scale bar: 10 μm.) (*B*) A cell has attached to the flat side of an opsonized ED and has spread on the particle. (Scale bar: 5 μm.) (*C*) An opsonized spherical particle has attached to the top of a cell, and the membrane has progressed over approximately half the particle. (Scale bar: 5 μm.) (*D–F*) Overlays of bright-field and fluorescent images after fixing the cells and staining for polymerized actin with rhodamine phalloidin. (*D*) Actin ring forms as remodeling and depolymerization enable membrane to progress over an opsonized ED by new actin polymerization at the leading edge of the membrane. (*E*) Actin polymerization in the cell at site of attachment to flat side of an opsonized ED, but no actin cup or ring is visible. (*F*) Actin cup surrounds the end of an opsonized sphere as internalization begins after attachment. (Scale bars in *D–F*: 10 μm.) At least five cells were observed for each orientation of each particle. Similar results were observed in all repetitions.

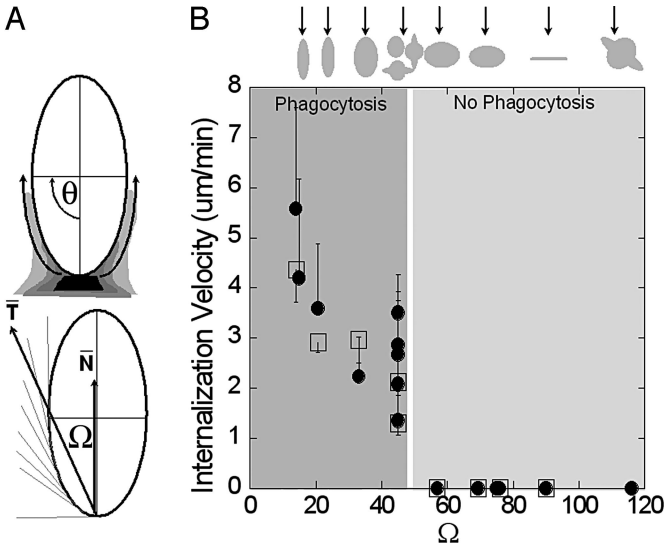

Fig. 4. Definition of Ω and its relationship with membrane velocity. (*A*) A schematic diagram illustrating how membrane progresses tangentially around an ED. $\bar{\mathbf{T}}$ represents the average of tangential angles from $\theta = 0$ to $\theta = \pi/2$. Ω is the angle between $\bar{\mathbf{T}}$ and membrane normal at the site of attachment, $\bar{\mathbf{N}}$. (*B*) Membrane velocity (distance traveled by the membrane divided by time to internalize, $n \geq 3$; error bars represent SD) decreases with increasing Ω for a variety of shapes and sizes of particles. Nonopsonized particles are indicated by filled circles, and IgG-opsonized particles are indicated by open squares. Each data point represents a different shape, size, or aspect ratio particle. The internalization velocity is positive for $\Omega \leq 45°$ ($P < 0.001$). Above a critical value of Ω, $\approx$45°, the internalization velocity is zero ($P < 0.001$) and there is only membrane spreading after particle attachment, not internalization. The arrows above the plot indicate the point of attachment for each shape that corresponds to the value of Ω on the *x* axis. Error in Ω is due to the difference in the actual point of contact in time-lapse microscopy from that used to calculate Ω. Only points of contact within 10° of that used to calculate Ω were selected. All data points at the critical point, $\Omega = 45°$, except UFOs, do not have error associated with Ω because of their symmetry.

tangents drawn to the target contour from the point of initial contact to the center line of the target (Fig. 4*A*).

$$\Omega = \cos^{-1}(\bar{\mathbf{N}}\cdot\bar{\mathbf{T}}) = \left\langle \int_0^{\theta} \frac{\mathbf{ds}}{\mathbf{d}\theta}\,\kappa(\theta)\mathbf{d}\theta \right\rangle_{0,\pi/2},$$

where $\kappa(\theta)$ is curvature and $\mathbf{ds}/\mathbf{d}\theta$ is the angular gradient of the arc length (see http://mathworld.wolfram.com/Ellipse.html). $\theta = 0$ is defined as the point of contact. Ω, evaluated numerically for each case, is a dimensionless parameter and depends only on the particle's shape and its point of attachment to the macrophage. It indicates the mean angle made by the membrane with $\bar{\mathbf{N}}$ as it travels around the particle during phagocytosis. For each attachment site on a particle, there exist two values of Ω defined for two orthogonal views of the particle, the larger of which is used in further analysis. For spheres of all sizes, the dome or ring of UFOs, and the edge of oblate ellipsoids, $\Omega = 45°$. For an ED with a major axis *a*, minor axis *b*, and relatively small thickness, $\Omega \sim \arctan(b/a)$ for a particle attaching along the major axis (Fig. 2*A*), $\Omega \sim \arctan(a/b)$ for attachment along the minor axis, and $\Omega \approx 90°$ for a cell attaching on the flat side (Fig. 2*B*). For the concave region of a UFO, $\Omega > 90°$. Because Ω depends only on particle shape, dependence of phagocytosis on size and shape can be clearly separated and understood.

Dependence of the rate of phagocytosis on Ω can be clearly seen in Fig. 4*B* where internalization velocity [total distance traveled by macrophage membrane to complete phagocytosis, evaluated in the 2D projected view of the particle (Fig. 4*A*), divided by the time required to complete phagocytosis] is plotted against Ω. Phagocytosis velocity decreased with increasing Ω. Furthermore, there was an abrupt transition in internalization velocity to zero at $\Omega \sim 45°$. Zero velocity is assigned when phagocytosis is not completed within the period of observation (2 h). Any lack of internalization in Fig. 4*B* is not due to particle size because all particles in this figure were successfully internalized from at least one attachment orientation. IgG-coated particles exhibited the same Ω-dependence as nonopsonized particles, confirming the generality of the dependence of phagocytosis on particle shape.

The sudden transition from phagocytosis to spreading at $\Omega \sim 45°$ is rather striking. Particles with $\Omega > 45°$ induced significant spreading of cells (for example, Fig. 3*B*) but not internalization. Spreading has been likened to "frustrated" phagocytosis, and phagocytosis has even been proposed as a simple model for spreading because many of the same proteins are involved in both processes (17–19). In fact, the leading membrane edge during phagocytosis in Figs. 3 *A–C* visually appears very much like that of a cell spreading on a flat surface. Apparent similarities between the two have led researchers to believe that cells cannot distinguish target shape (7). However, the observations described here show a significant difference in the features of actin remodeling during phagocytosis and simple spreading. Although actin is present at the membrane–particle interface in both cases, formation of an actin cup and ring, clearly visible during phagocytosis, is absent during spreading. More importantly, the fine line between phagocytosis and spreading is defined by the shape of the particle from the cell's perspective,

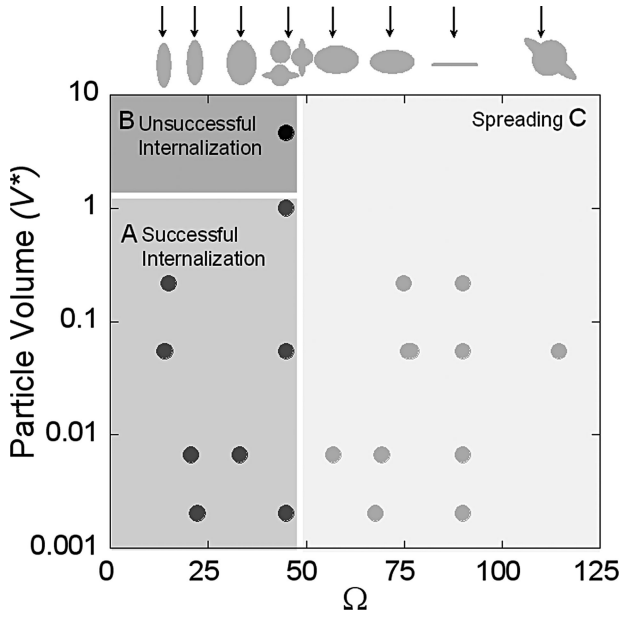

Fig. 5. Phagocytosis phase diagram with Ω and dimensionless particle volume V^* (particle volume divided by 7.5 μm radius spherical cell volume) as governing parameters ($n = 5$ for each point). Initialization of internalization is judged by the presence of an actin cup or ring as described in the text. There are three regions. Cells attaching to particles at areas of high Ω, >45°, spread but do not initiate internalization (region C). Cells attaching to particles at areas of low Ω, <45°, initiate internalization (regions A and B). If V^* is ≤1, internalization is completed (region A). If $V^* > 1$, internalization is not completed because of the size of the particle (region B). The arrows above the plot indicate the point of attachment for each shape that corresponds to the value of Ω on the *x* axis. Each case was classified as phagocytosis or no phagocytosis if >95% of observations were consistent. Each data point represents a different shape, size, or aspect ratio particle.

Ω. This conclusion is brought out by the use of particles of various shapes, a feature that was not present in previous studies on this topic (2–7).

The overall process of phagocytosis is a result of the complex interplay between shape and size (Fig. 5). This phase diagram shows whether or not internalization was initialized and completed for particles with different combinations of Ω and V^*, the ratio of particle volume to macrophage volume. Initiation of internalization was judged by formation of an actin cup or ring (Fig. 3 *D* and *F*), and completion was judged by closure of the membrane. The diagram shows three regions: the successful phagocytosis region ($\Omega \leq 45°$, $V^* \leq 1$) where phagocytosis is initiated and completed quickly, the attempted phagocytosis region ($\Omega \leq 45°$, $V^* > 1$) where phagocytosis is initiated but not completed within the period of observation, and the spreading region ($\Omega > 45°$) where particle attachment takes place and macrophages spread on the particle but phagocytosis is not initiated. This diagram clearly shows that initiation of phagocytosis is governed by Ω whereas V^* primarily influences completion. Macrophages phagocytosed particles as large as themselves when approached from the preferred orientation ($\Omega \leq 45°$). However, when approached from the undesired orientation ($\Omega > 45°$), they did not internalize particles with volumes as small as 0.2% of the cell volume. Similar bias has also been seen during phagocytosis of pathogens based on limited anecdotal literature (see *Supporting Discussion*, which is published as supporting information on the PNAS web site). It remains to be seen whether the orientation bias of phagocytosis disappears at extremely small particle volumes ($V^* \ll 0.002$).

The mechanism for shape dependence of phagocytosis requires further examination. Because the formation of a coordinated actin cup is crucial to initializing phagocytosis, it is likely that the dynamics of actin remodeling play a central role in the shape dependence of phagocytosis. As the membrane surrounds a particle during phagocytosis, the circumference of the actin ring (Fig. 3*D*) follows the local geometry of the particle. During early stages of phagocytosis the ring expands to surround the particle on all sides and the magnitude of expansion necessary to surround a certain length of the particle increases with increasing Ω. Because actin remodeling is a metabolically intensive process, it is likely that particles that require only gradual expansion of actin ring (that is, particles with low Ω) are phagocytosed more effectively. In fact, closer inspection of the macrophage in Fig. 2*A* (and see Movie 1) reveals that, even within the same particle, the time required for the cell to internalize the middle third of an ED (region of relatively constant circumference) is half of that required to internalize the first third of the ED (region of expanding circumference). Beyond a certain value of Ω, the magnitude of expansion necessary to form an actin cup may inhibit phagocytosis completely.

These results provide a paradigm for analyzing phagocytosis of natural targets that inherently exhibit geometric anisotropy. Size plays a much different role in phagocytosis than originally thought. Cells are not able to detect macroscopic properties such as volume until phagocytosis is complete. Accordingly, initiation of internalization is independent of the physical dimensions of the particles. Ultimately, however, the size of the particle could prevent the cell from successfully completing internalization. Understanding of the complex interplay between shape and size presented in this study is essential to fully elucidating phagocytosis of natural targets. Unexpectedly, the use of particles with various shapes also shed light on similarities and differences between phagocytosis and spreading. Although similar processes, ultimately the shape of the surface at the point of initial contact dictates which one cells undergo. This is a remarkable example of cell behavior being dictated by the physical environment (20), which is often overlooked. Particles described here could be used for further fundamental studies on cell motility, spreading, and phagocytosis to gain new insights into their mechanisms. In addition, understanding the role of shape in phagocytosis opens up exciting possibilities in engineering drug delivery carriers to either avoid (21) or promote (22) phagocytosis.

Materials and Methods

Particle Preparation. Uncrosslinked PS spherical particles (radii 1–12.5 μm) were purchased from Polysciences. All chemicals used were of commercial grade. Fully hydrolyzed poly(vinyl alcohol) (PVA) was purchased from Sigma. The protocol used for fabrication of nonspherical particles was adapted from Ho *et al.* (8). Specifically, 5–10% PVA (2–4 g in 40 ml of water) was dissolved in 75°C water, depending on the desired film thickness. Two percent glycerol was added to plasticize the films. Spherical particles were added to this mixture to a concentration of 0.04% wt/vol, and the films were dried on a 19 × 27-cm flat surface to a thickness of 35 μm for 5% PVA and 70 μm for 10% PVA. The films were then stretched in one or two directions by using a custom-made apparatus. Particle dimensions were controlled by the amount of stretching imposed on the film. Particle volume was controlled by the diameter of sphere initially used. The exact conditions and stretching ratios used to create each geometry are described in Table 1 and Fig. 6 (which are published as supporting information on the PNAS web site). Stretching took place either at 120°C in an oil bath (above the glass transition temperature of PS) or after soaking in toluene for 3 h. In the case where the film was stretched under high temperatures, the film

was allowed to cool to room temperature. When toluene was used during stretching, the film was dried at room temperature for 24 h on the stretching apparatus and soaked in isopropanol for 24 h to extract any remaining toluene still in the particles. The films were dissolved in 30% isopropanol/water at 65°C. The particles were washed by centrifugation with the same solution 10 times to remove all PVA from the surface of the particles. To verify particle morphology, particles were coated with palladium (Hummer 6.2 sputtering system; Anatech, Union City, CA) and imaged with the Sirion 400 scanning electron microscope (FEI, Hillsboro, OR) at 3 eV. Particle dimensions were measured from the micrographs with METAMORPH image acquisition and analysis software (Universal Imaging, Downingtown, PA). For opsonization, particles were incubated with 0.25 mg/ml rabbit IgG (Sigma) for 30 min at 37°C. The particles were washed twice with PBS. Opsonization was verified with fluorescently tagged IgG (Molecular Probes).

Cells. Continuous alveolar rat macrophage cells NR8383 (American Type Culture Collection) were used as model macrophages. Mouse peritoneal macrophage cells J774 were also used to verify the generality of results among macrophage populations of different species and tissues. Both cell types were cultured in F-12K media (American Type Culture Collection) supplemented with 10% heat-inactivated FBS and 1% penicillin/streptomycin (Sigma) under standard culture conditions (37°C, 5% CO_2, humidified). To ensure that macrophages were capable of spreading, cells were incubated on plain and IgG-coated coverslips and viewed with phase contrast light microscopy to identify circular spread cells.

Time-Lapse Video Microscopy. Cells (2×10^5 cells per ml) were allowed to attach in dishes lined with coverslip glass in F-12K media supplemented with 10% FBS and 25 mM Hepes (Sigma). The dishes were placed on an Axiovert 25 microscope (Zeiss) at $\times 100$ with phase contrast filters and equipped with the Delta T controlled culture dish system (Bioptechs, Butler, PA) to keep the cells at 37°C. Particles (one particle per cell) were added to the dishes, and bright-field images were collected every 30 seconds for 2 h by a CoolSNAP HQ charge-coupled device camera (Roper Scientific) connected to the METAMORPH software. In some cases, cells were observed for 12 h and cell behavior was the same as for 2 h. Observed cells were randomly chosen from the entire population, thus discounting potential bias due to heterogeneity in macrophage size (radius 7.5 ± 2.5 μm). Images were condensed into movies and analyzed manually for phagocytic events. Successful phagocytosis exhibited membrane ruffling at the site of attachment, blurring the crisp boundary of the membrane, and subsequent reforming of the membrane boundary after internalization. The method of visual scoring of phagocytosis was validated for IgG-opsonized particles by using Alexa Fluor monkey anti-rabbit secondary fluorescent antibody (Molecular Probes) that bound to rabbit IgG on particles when they were not internalized. Phagocytic events were also verified by using scanning electron microscopy and actin staining. Phagocytosis was analyzed based on internalization of one attached particle by a single cell.

Scanning Electron Microscopy. Scanning electron microscopy was used for high-magnification confirmation of cell membrane progression on the particles at various times during internalization. After 7–60 min of incubation with particles at 37°C, cells were fixed with 2% electron microscopy-grade glutaraldehyde (Electron Microscopy Sciences). They were washed with serial dilutions of water and ethanol, dried under vacuum, and coated with palladium (Hummer 6.2 sputtering system). Cells were imaged with the Sirion 400 scanning electron microscope at 2 eV.

Actin Staining. Cells were allowed to attach in dishes as in time-lapse video microscopy. Particles were added to the dishes and incubated at 37°C for 10 or 120 min. The cells were fixed with 4% electron microscopy-grade paraformaldehyde (Electron Microscopy Sciences) for 30 min. Once fixed, the cells were washed with PBS and permeabilized with 0.1% Triton X-100 (ICN) for 3 min. The cells were washed again with PBS, and 2.5 units/ml rhodamine phalloidin (Molecular Probes) was added to each dish for 15 min to stain polymerized actin filaments. The dishes were washed with PBS and viewed at $\times 100$. Bright-field and fluorescent images of cells with a single attached particle were acquired and overlayed. Cells were inspected manually for the presence of a fluorescent actin cup or ring as described above.

We thank Tuan Dinh for many discussions, Andy Weinberg for machining the stretching devices, and Duane Sears for mouse peritoneal macrophages. This work was supported by a grant from the University of California Biotechnology Research and Education Program and partially supported by the Materials Research Science and Engineering Centers program of the National Science Foundation. J.A.C. was supported by a fellowship from the National Science Foundation.

1. Aderem, A. & Underhill, D. M. (1999) *Annu. Rev. Immunol.* **17,** 593–623.
2. Simon, S. I. & Schmidschonbein, G. W. (1988) *Biophys. J.* **53,** 163–173.
3. Tabata, Y. & Ikada, Y. (1988) *Biomaterials* **9,** 356–362.
4. Kawaguchi, H., Koiwai, N., Ohtsuka, Y., Miyamoto, M. & Sasakawa, S. (1986) *Biomaterials* **7,** 61–66.
5. Rudt, S. & Muller, R. H. (1992) *J. Controlled Release* **22,** 263–271.
6. Koval, M., Preiter, K., Adles, C., Stahl, P. D. & Steinberg, T. H. (1998) *Exp. Cell Res.* **242,** 265–273.
7. Cannon, G. J. & Swanson, J. A. (1992) *J. Cell Sci.* **101,** 907–913.
8. Ho, C. C., Keller, A., Odell, J. A. & Ottewill, R. H. (1993) *Colloid Polym. Sci.* **271,** 469–479.
9. Lu, Y., Yin, Y. D. & Xia, Y. N. (2001) *Adv. Mater.* **13,** 271–274.
10. O'Brien, D. K. & Melville, S. B. (2003) *Microbiology* **149,** 1377–1386.
11. Kobzik, L., Huang, S. L., Paulauskis, J. D. & Godleski, J. J. (1993) *J. Immunol.* **151,** 2753–2759.
12. Palecanda, A., Paulauskis, J., Al-Mutairi, E., Imrich, A., Qin, G. Z., Suzuki, H., Kodama, T., Tryggvason, K., Koziel, H. & Kobzik, L. (1999) *J. Exp. Med.* **189,** 1497–1506.
13. May, R. & Machesky, L. (2001) *J. Cell Sci.* **114,** 1061–1077.
14. Lee, E. Y., Pang, K. M. & Knecht, D. (2001) *Biochim. Biophys. Acta* **1525,** 217–227.
15. Aizawa, H., Fukui, Y. & Yahara, I. (1997) *J. Cell Sci.* **110,** 2333–2344.
16. Lee, E., Shelden, E. A. & Knecht, D. A. (1997) *Exp. Cell Res.* **235,** 295–299.
17. Cougoule, C., Wiedemann, A., Lim, J. & Caron, E. (2004) *Semin. Cell Dev. Biol.* **15,** 679–689.
18. Welch, M. D. & Mullins, R. D. (2002) *Annu. Rev. Cell Dev. Biol.* **18,** 247–288.
19. Castellano, F., Chavrier, P. & Caron, E. (2001) *Semin. Immunol.* **13,** 347–355.
20. Beningo, K. A. & Wang, Y. L. (2002) *J. Cell Sci.* **115,** 849–856.
21. Dalhaimer, P., Engler, A. J., Parthasarathy, R. & Discher, D. E. (2004) *Biomacromolecules* **5,** 1714–1719.
22. Foged, C., Brodin, B., Frokjaer, S. & Sundblad, A. (2005) *Int. J. Pharm.* **298,** 315–322.